ЖЭТФ, 2013, том 144, вып. 3 (9), стр. 632–652 © 2013

GIANT MAGNETORESISTANCE IN THE VARIABLE-RANGE HOPPING REGIME

L. B. Ioffe [a,b*], ***B. Z. Spivak*** [c]

[a] *LPTHE, Université Pierre et Marie Curie, Paris CEDEX 05, France*

[b] *Department of Physics, Rutgers University New Jersey, 08854, USA*

[c] *Department of Physics, University of Washington Seattle, WA 98195, USA*

Received May 3, 2013

Dedicated to the memory of Professor Anatoly Larkin

We predict the universal power-law dependence of the localization length on the magnetic field in the strongly localized regime. This effect is due to the orbital quantum interference. Physically, this dependence shows up in an anomalously large negative magnetoresistance in the hopping regime. The reason for the universality is that the problem of the electron tunneling in a random media belongs to the same universality class as the directed polymer problem even in the case of wave functions of random sign. We present numerical simulations that prove this conjecture. We discuss the existing experiments that show anomalously large magnetoresistance. We also discuss the role of localized spins in real materials and the spin polarizing effect of the magnetic field.

DOI: 10.7868/S0044451013090149

1. INTRODUCTION

In strongly disordered conductors, single electrons states are localized, and therefore the conductivity is due to phonon-assisted electron tunneling between localized states. The length of a typical hop r_{hop} increases as the temperature is decreased and becomes much larger than the distance between the localized states in the variable-range hopping regime [1, 2]. In this paper, we study the orbital mechanism of the magnetoresistance in this regime. We show that at sufficiently low temperatures, it is due to the localization length dependence on the magnetic field B and that it is given by a universal power law. This localization length dependence on the magnetic field translates into an exponentially large variation of the resistance. The sign of the orbital magnetoresistance depends on the details of impurity scattering, but in the typical case, the low-temperature magnetoresistance is negative. Similarly to the metallic regime, the origin of the negative magnetoresistance is the electron quantum interference, but the amplitudes that interfere correspond to different processes in these two cases. Despite its much larger magnitude, the negative magnetoresistance in the hopping regime received much less attention, both theoretically and experimentally, than its counterpart in the metallic regime. One of the goals of this paper is to draw the attention of the community to this interesting phenomenon.

We begin with a brief review of the nature of magnetoresistance in metals. The conventional theory of magnetoresistance associates it with the classical effect of electron motion along cyclotron orbits. For a typical metal, the magnetoresistance is controlled by the parameter $(\omega_c\tau_{tr})^2$, where ω_c is the cyclotron frequency and τ_{tr} is the transport mean free time (see, e. g., [3]). In contrast to these expectations, many disordered metals show negative magnetoresistance at small magnetic fields. The negative magnetoresistance in weakly disordered metals has been explained in the framework of the weak localization theory, which takes into account the quantum interference of probability amplitudes for electrons to travel along self-intersecting

*E-mail: ioffe@physics.rutgers.edu

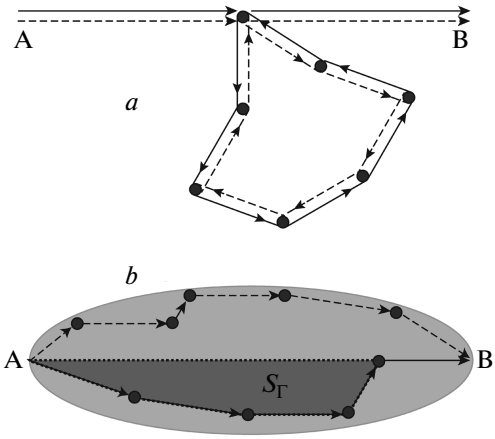

Fig. 1. Qualitative picture of the interference effects in disordered metals. Panel a shows interference in the weak localization regime that is due to self-crossing diffusive paths. Quantum propagation from A to B is the sum of two amplitudes that contain clockwise and counterclockwise motion along the loop that is a part of the self-intersecting path. Panel b shows interference in the hopping regime in which the backward motion of electrons gives negligible contribution to the tunneling between sites A and B. In this case, typical paths contributing to the interference are located in the shaded (light gray) area with the transverse direction that scales with the length of the hop L. The magnetic field has a significant effect if the flux S_Γ through the area formed by a typical path and a straight line (dark gray) is of the order of one flux quantum

diffusive paths [4–7], such as those shown in Fig. 1*a*. The interfering amplitudes correspond to the clockwise and counterclockwise propagation of the electron wave along the loop formed by a self-intersecting path. In the absence of the magnetic field, these amplitudes interfere constructively, increasing the probability of return to the intersection point. In the presence of the magnetic field, these amplitudes acquire different phases, and the interference is suppressed, leading to the negative magnetoresistance. The negative magnetoresistance magnitude in this regime is relatively small because it scales with the small parameter $1/k_F l_{tr}$, where k_F is the Fermi momentum and l_{tr} is the transport mean free path.

Experimentally, in many materials the magnetoresistance in the hopping regime is significantly larger than in the metallic regime. A positive magnetoresistance of several orders of magnitude in the hopping regime has been observed long ago (see, e. g., Ref. [1] and the references therein). Significant negative magnetoresistance in the variable-range hopping regime ranging up to two orders of magnitude has been observed in many experimental works [8–18]. In some of these works, a large anisotropy of the negative magnetoresistance has been observed in $2D$ samples, indicating its orbital nature.

Phonon emission and absorption make different hopping events incoherent, while the electron tunneling between localized states is a quantum mechanical process. The magnetoresistance is due to the magnetic field dependence of the probability of one hop. Qualitatively, large orbital magnetoresistance in the hopping regime is due the interference of the tunneling amplitudes along different tunneling paths contributing to a single hop that are distributed in a cigar-shaped region shown in Fig. 1*b*. In this regime, the tunneling paths containing loops give exponentially small contribution to the tunneling probability. This is the main difference from the weak localization, where the interference is due to the paths that circle a loop (see Fig. 1*a*). In the variable-range hopping regime, electrons hop over distances much larger than the distance between localized states, and hence the cigar-shaped region contains many electron scatterers. The amplitude μ_i describing the individual scattering process at a state i can be positive and negative. The sign distribution of the μ_i determines the sign of the magnetoresistance, as we explain below in Sec. 2.3.

Large positive magnetoresistance may be associated with a shrinkage of the hydrogen-like localized electron wave functions at the scales less than the inter-impurity distance. Quantitatively, this picture works well only in a very high magnetic field and at sufficiently high temperatures at which the typical electron hopping length is shorter than the distance between impurities. A theory of the positive magnetoresistance that takes the electron scattering with positive scattering amplitudes into account has been developed in [19–23]. In this case, the tunneling amplitudes interfere constructively in the absence of the field, while the phases induced by the magnetic field destroy this interference.

An orbital mechanism of the negative magnetoresistance may be associated with the randomness of the signs of the scattering amplitudes μ_i, which is due to the random sign of $\epsilon - \epsilon_i$ [24–29]. Here, ϵ is the energy of the tunneling electron and ϵ_i is the energy of a localized state. This sign randomness may lead to random signs of the interfering tunneling amplitudes at $B = 0$. The magnetic field makes tunneling amplitudes complex, which increases the conductance in this situation. Thus, the sign of the orbital magnetoresistance is related to the sign distribution of the localized electron wave functions.

In this paper, we develop a quantitative theory of orbital magnetoresistance in the hopping regime and discuss the available experimental data in the light of our results. Because most of experiments have been done on two-dimensional samples, we focus on the two-dimensional hopping regime of electrons and the corresponding experiments.

We show that in physically relevant cases, even a small concentration of impurities with $\mu_i < 0$ leads to completely random signs of the tunneling amplitudes at large scales. Therefore, at sufficiently low temperatures and small magnetic fields, the variable-range hopping magnetoresistance is negative. At higher magnetic fields and higher temperatures, it can be both positive and negative.

The plan of the paper is as follows. In Sec. 2.1, we start with a brief review of the basis of variable-range hopping theory and discuss a qualitative picture of the variable-range hopping magnetoresistance. In Secs. 2.2 and 2.3, we discuss the statistics of the modulus and the sign of the localized electron wave function. In particular, in Sec. 2.3, we discuss the conditions for the existence of the "sign phase transition", where as a function of the concentration of scatterers with $\mu_i < 0$, the system changes from the sign-ordered to sign-disordered phases. In Sec. 3, we apply the theory developed in Sec. 2 to compute the magnetoresistance. Section 4 discusses applications of the results for the sign phase transition to other physical systems. Finally, Sec. 5 gives a short review of the experimental situation.

2. ELECTRON TRANSPORT IN THE VARIABLE-RANGE HOPPING REGIME

2.1. Review of the variable-range hopping theory

In the localized regime, the electron wave functions decay exponentially with the distance $|\mathbf{r} - \mathbf{r}_i|$ from the impurity: $\psi_i(\mathbf{r}) \sim \exp(-|\mathbf{r} - \mathbf{r}_i|/\xi)$, where $\mathbf{r}_i$ is the center of a localized wave function and ξ is a typical localization radius. In this case, the conductivity is determined by phonon-assisted electron hopping between localized states. At low temperatures, the typical hopping length r_{hop} is determined by the competition between two exponential factors: the hopping probability W_{ij} that decays exponentially with the distance r_{ij} between impurities and the thermal factor $\exp(-E_{hop}(r_{ij})/T)$, where $E_{hop}(r_{ij})$ is the hopping activation energy that decreases with r_{ij}. These factors give the exponential dependence of the typical hopping rate at a distance r_{hop}: $\exp(-E_{hop}(r)/T - 2r/\xi)$. This exponential factor is maximal for the typical hopping length r_{hop}, which is much larger than the distance between localized states, as illustrated in Figs. 1*b*, 2:

$$r_{hop} \sim \left(\frac{T_0}{T}\right)^{\zeta} \xi. \tag{1}$$

As a result, the resistivity acquires an exponential dependence on temperature [1, 2]:

$$\rho(T) = \rho_0 \exp\left[-\left(\frac{T_0}{T}\right)^{\zeta}\right]. \tag{2}$$

Here, the prefactor ρ_0 is determined by the electron–phonon matrix element and ξ is the localization radius.

Generally, the density of localized states can be energy-dependent near the Fermi energy [1]:

$$\nu(\epsilon) = C\epsilon^{\beta}, \tag{3}$$

where we count the energy ϵ of a tunneling electron from the Fermi energy. In the absence of electron–electron interaction (Mott's theory), the density of states at the Fermi level is constant ($\beta = 0$ and $C = \nu_0$), leading to the activation energy $T_0 \approx 13(\nu_0\xi^2)^{-1}$ and to the exponent $\zeta = 1/3$ for $d = 2$ (Mott's law). In the case where electrons (in two or three dimensions) interact via the three-dimensional Coulomb interaction (Efros–Shklovskii regime) $\beta = 1$, $C \approx (2/\pi)\, e^4/\kappa^2$, where κ is the dielectric constant. This results in $\zeta = 1/2$ and $T_0 \sim e^2/\kappa\xi$ for $2D$ electrons with the three-dimensional Coulomb interaction.

The qualitative arguments of the Mott theory can be made more quantitative by considering the percolating cluster of electron hops [1]. Probability of a single hop between the states localized around positions r_i and r_j is given by

$$W_{ij} = \frac{2\pi}{h} \int |M_{ij}(\mathbf{q})|^2 \delta(\epsilon_i - \epsilon_j - uq)\, d^d q, \tag{4}$$

where

$$M_{ij} \sim \int d^d\mathbf{r}\, \psi_i(\mathbf{r} - \mathbf{r}_i)\, \psi_j(\mathbf{r} - \mathbf{r}_j)\, e^{i\mathbf{q}\cdot\mathbf{r}} \tag{5}$$

is the phonon matrix element, u is the speed of sound, and $\mathbf{q}$ is its wave vector. Because the wave functions $\psi_i(\mathbf{r} - \mathbf{r}_i)$ and $\psi_j(\mathbf{r} - \mathbf{r}_j)$ decrease exponentially, M_{ij} and W_{ij} are exponential functions of the localization length $\xi(B)$.

In the main part of this paper, we consider the magnetic field range in which the $W_{ij}(B)$ dependence is dominated by $\xi(B)$. In this case, we can approximate the phonon tunneling matrix element by the amplitude of tunneling between states i and j: $M_{ij} \sim A_{ij}$.

In a uniform medium, the magnetic field suppresses the amplitude of a single quantum tunneling event:

$$A_{ij} \propto \exp\left(-\frac{r_{ij}^2}{2L_B^2}\right) \quad \text{at} \quad r_{ij} \gg \frac{L_B^2}{\xi}, \tag{6}$$

which gives positive magnetoresistance. Here, $L_B = (c\hbar/eB)^{1/2}$is the magnetic length. In disordered media, electrons scatter from other localized states that have energies different from the energy of the final state. The effect of the magnetic field is due to the interference of the directed optimal paths, which is shown schematically in Fig. 1*b*. In this case, $A_{if} = \sum_\Gamma A_\Gamma$ is a coherent sum of amplitudes $A_\Gamma(B)$ to tunnel along paths Γ between the initial "i" and final "f" sites. The tunneling paths can be defined by the sequence of states that scatter electrons in the course of tunneling. At zero magnetic field $\mathbf{B} = 0$, the wave functions of localized states and the tunneling amplitudes $A_\Gamma(0)$ can be chosen to be real [30]:

$$\begin{aligned} A_{if}(0) = {} & \frac{1}{|\mathbf{r}_f - \mathbf{r}_i|^{1/2}} \exp\left(-\frac{|\mathbf{r}_j - \mathbf{r}_i|}{\xi}\right) + \\ & + \sum_\alpha \frac{1}{|\mathbf{r}_\alpha - \mathbf{r}_i|^{1/2}} \exp\left(-\frac{|\mathbf{r}_\alpha - \mathbf{r}_i|}{\xi}\right) \times \\ & \times \frac{(\mu_\alpha)^{1/2}}{|\mathbf{r}_\alpha - \mathbf{r}_j|^{1/2}} \exp\left(-\frac{|\mathbf{r}_\alpha - \mathbf{r}_f|}{\xi}\right) + \\ & + \sum_{\alpha,\beta} \frac{1}{|\mathbf{r}_\alpha - \mathbf{r}_i|^{1/2}} \exp\left(-\frac{|\mathbf{r}_\alpha - \mathbf{r}_i|}{\xi}\right) \frac{\mu_\alpha}{|\mathbf{r}_\beta - r_\alpha|^{1/2}} \times \\ & \times \exp\left(-\frac{|\mathbf{r}_\beta - \mathbf{r}_\alpha|}{\xi}\right) \frac{\mu_{\beta,}}{|\mathbf{r}_\beta - \mathbf{r}_f|^{1/2}} \times \\ & \times \exp\left(-\frac{|\mathbf{r}_\beta - \mathbf{r}_f|}{\xi}\right) + \ldots = \end{aligned} \tag{7}$$

$$= \sum_\Gamma A_\Gamma(0), \tag{8}$$

$$\mu_\alpha \sim \frac{b}{\epsilon_\alpha - \epsilon_i}. \tag{9}$$

Here, μ_α is the amplitude of scattering on α's localized state, ϵ_i and ϵ_α are energies of the tunneling electron and the localized scattering state, $b \sim \sqrt{\xi}\epsilon_0 > 0$, and ϵ_0 is the characteristic binding energy of the localized states. Generally, ϵ_α are random quantities, and hence the amplitudes $A_\Gamma(\mathbf{B} = 0) = A_\Gamma(0)$ have random signs. We note that Eq. (7) describes both the processes in which an electron is scattered by empty sites and the processes in which it goes through occupied sites (see Fig. 2), which can be described as a hole moving backwards. The important condition for the interference is that in the final state, all intermediate electrons should return to their original positions and spin states.

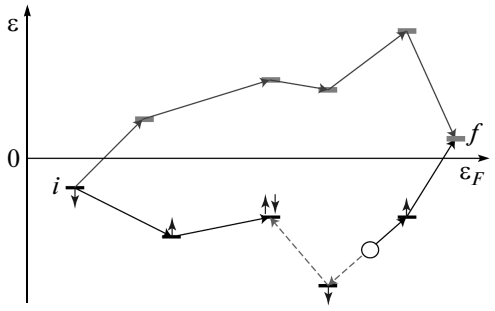

Fig. 2. Qualitative picture of the phonon-assisted tunneling through localized states from the initial state i to the final state f. Solid bars indicate the energies of the localized states. The energies of the initial and final states are close to the Fermi energy $\epsilon_F = 0$ (indicated by the dashed line) while the intermediate localized states are typically farther away from $\epsilon = 0$. The states with negative energies can be filled with one or two electrons. In the former case, they are characterized by the spin of the electron shown by vertical arrows. The states with $\epsilon > 0$ are empty. Black and gray arrows indicate electron tunneling paths through empty and filled localized states. If the path goes through a site that is already occupied by the electron with the same spin, the coherent process occurs by creating an electron–hole pair (indicated by the empty circle), then by tunneling the hole carrying the opposite spin in the opposite direction, and finally by anihilating it with the electron coming from the left. This process leaves the spin state intact. The incoherent process in which the hole carrying the same spin might also be possible in some physical situations (see Sec. 3.3)

The hopping probability W_{if} is a random quantity. Generally, to obtain the value of the resistance of the system, one has to solve the full percolation problem with the probability of individual hops given by W_{if} [1]. But as long as

$$\ln\frac{\rho(B)}{\rho(0)}\frac{1}{\ln\rho(0)} \ll 1,$$

the magnetoresistance is given by the average of the logarithm of the hopping probability [1]:

$$\ln\frac{\rho(B)}{\rho(0)} = -\left\langle \ln\frac{W_{if}(B)}{W_{if}(0)} \right\rangle. \tag{10}$$

Here, the brackets denote averaging over random scattering configurations and over different hoppings that belong to a percolation cluster. These hoppings are characterized by a typical hopping length r_{hop}. With a good accuracy, we can replace the full average (10) with the average over random scattering configurations for

the hopping processes by the distance r_{hop}. Physically, the averaging of the logarithm in (10) means that the resistivity is controlled by the typical hopping probability rather than by rare events.

The application of a magnetic field $\mathbf{B}$ introduces random phases to the tunneling amplitudes,

$$A_\Gamma(B) = A_\Gamma(0) \exp\left(i2\pi \frac{\Phi_\Gamma}{\Phi_0}\right), \qquad (11)$$

where $\Phi_\Gamma = BS_\Gamma$ and S_Γ is the area enclosed between the the path Γ and the straight line going from the initial to final states (see Fig. 1*b*).

Depending on distributions of the signs of the amplitudes $A_\Gamma(0)$, the orbital magnetoresistance can be both positive and negative. To illustrate this fact, we consider a model in which there are only two paths, $A_1(0) \sim A_2(0)$, which are independent random quantities and $|\Phi_1 - \Phi_2| \sim \Phi_0$. If $A_{1,2}(0) > 0$ are positive, in the presence of magnetic field, then the amplitudes $A_\Gamma(B)$ partially cancel each other. As a result, $\langle \ln W_{ij}(B)\rangle$ decreases by a factor of the order of unity when $|\Phi_1 - \Phi_2| \sim \Phi_0$. In this case, the magnetoresistance is positive.

The situation changes if $A_{1,2}(0)$ have random signs. In the simplest case where the signs are completely random, the average probability

$$\left\langle \left| \sum A_\Gamma(B) \right|^2 \right\rangle = \sum \left\langle |A(0)|^2 \right\rangle$$

is independent of $\mathbf{B}$. If the magnetic flux through the closed loop formed by paths 1 and 2 is larger than the flux quantum, the phases of the amplitudes $A_{1,2}$ are completely random, and therefore $\langle A_1(B)A_2(B)\rangle = 0$. This implies that the variance

$$\left\langle \left| \sum_\Gamma A_\Gamma(B) \right|^4 \right\rangle - \left\langle \left| \sum_\Gamma A_\Gamma(B) \right|^2 \right\rangle^2$$

decreases by a factor of the order of unity when $|\Phi_1 - \Phi_2| \sim \Phi_0$. As a result, a typical value of the resistance defined by (10) increases by a factor of the order of unity and the magnetoresistance is negative.

This simplified picture of magnetoresistance being determined by the interference between only two paths becomes more complicated for two reasons. First, at large scales, the propagation amplitude is dominated by many paths that go through the same scatterer or a group of scatterers. This implies strong correlations between the amplitudes A_Γ, as we discuss in Sec. 3.1. This makes the mathematical problem calculating $\rho(B)$ nontrivial. Second, the behavior of the magnetoresistance becomes more complicated if the amplitude signs are correlated at some finite distances (see Sec. 2.3). In this case, we can expect a crossover from the negative to positive magnetoresistance as the field increases, as we explain in Sec. 3.

Because the sign and the magnitude of the magnetoresistance are intimately related to the statistics of the sign and amplitude distribution of $A_{ij}(0)$, we start with a discussion of this quantity.

2.2. Statistics of the amplitude A in the absence of the magnetic field

In the case of small and positive scattering amplitudes $\mu_\alpha > 0$ and at zero magnetic field, the problem of electron tunneling can be mapped [30–33] onto the problem of directed polymers. In the latter problem, one studies the thermodynamics of an elastic string in a delta-correlated two-dimensional random potential $W(x, y)$, characterized by the energy functional

$$H_{dirpol}\{y(x)\} = \int_{-\infty}^{x} \left[\frac{\sigma}{2}(\partial_x y)^2 + W(x, y(x))\right] dx. \qquad (12)$$

Introducing the partition function

$$Z(y, x) = \sum_{y\{x\}} \exp(-\beta H)$$

of the string that ends at the point (x, y), we obtain that its evolution as a function of x is described by the equation

$$\partial_x Z = \frac{1}{2\beta\sigma}\partial_y^2 Z - \beta W(x, y)Z. \qquad (13)$$

This equation should be compared with the equation for the particle propagation in disordered media:

$$E\Psi = -\frac{1}{2m}\nabla^2\Psi + V(x, y)\Psi, \qquad (14)$$

with the white-noise potential $V(x, y)$. At negative energies corresponding to tunneling; after substitution

$$\Psi = \exp(-\beta\sigma x)Z(x, y)$$

we can neglect the terms with the second-order derivative in x, which are small at a weak potential $V \ll -E$. Then Schrödinger equation (14) coincides with (13) with $(\sigma\beta)^2 = -2mE$ and $W = \sigma V/2E$. This mapping also holds for an arbitrary (not necessarily white-noise correlated) potential V. However, it becomes less useful for arbitrary potentials because analytic results

for this problem were obtained only in the case of the white-noise potential.

Computation of positive magnetoresistance requires solving the directed polymer problem beyond the white noise approximation, and hence the analytic results are not directly applicable. Furthermore, the physically relevant problem of scattering with negative amplitudes cannot be mapped onto any thermodynamic problem because the corresponding free energy becomes imaginary. The applicability of the results of the directed polymer problem in the white noise approximation becomes even more questionable in this case. Below, we give a brief review of the results of the directed polymer problem in the white noise approximation. Then we present results of our numerical simulations beyond the white noise approximation, which indicate that these problems belong to the same universality class. Finally, we discuss the statistics of the signs of the tunneling amplitude and show that the existence of the "sign phase transition" is compatible with the results for the directed polymer problem.

The main result of the directed polymer theory is the scaling form of the fluctuational part of a free energy of a polymer of length L, $F \propto L^{1/3}$, and its deviations in the transverse direction $Y \propto L^{2/3}$. For the equivalent problem of domain wall pinning, this scaling was first found numerically in [34]. Analytically, it was extracted from the third moment of the distribution function of polymers of length L, $\mathcal{P}(F)$ [35, 36]. The replica method that was used in this work might be questioned because of an apparent noncommutativity of the limits $L \to \infty$ and $n \to 0$ and because it gives unphysical results for all moments of the distribution function except the third. All these problems can be eliminated by solving for the distribution of the energy differences of the infinitely long polymers that end at different points y_1 and y_2; this solution gives the same scaling exponents [37] as the original approach [34–36, 38–40].

The striking generality of this scaling result that we prove by numerical simulations below is, probably, due to the qualitative reasoning that relates it to the Markovian form of the free energy fluctuations as a function of the transverse coordinate. Indeed, the Markovian form implies that free energy fluctuations at large scales are proportional to $Y^{1/2}$; on the other hand, they should be of the order of the string elastic energy at these scales, $Y^2/L \propto Y^{1/2}$. Solving the last equation for Y gives the scaling dependences of the exact solution and of the numerical simulations.

Despite being intuitively appealing, the Markovian nature of free energy fluctuations is difficult to prove for the physically relevant situation in which some scattering amplitudes (9) are very large. It is even more difficult to prove it in the case of negative scattering amplitudes in which wave function can change sign at some points. At these points, the free energy defined by $F \equiv -T \ln Z$ acquires an imaginary part ($\operatorname{Im} F = \pi$) while its real part becomes large. Because these points are due to close by negative scatterers, the effective free energy becomes highly correlated, which violates the main assumption of the Markovian nature of the free energy fluctuations.

Recently [41, 42], a full Bethe-ansatz solution of problem (12) established the complete form of the distribution function of the free energy $F \equiv -T \ln Z$ of the string of length L, which turns out to coincide with the Tracy–Widom distribution [43]. This result allows us to check that the problem of particle hopping belongs to the same universality class as the directed polymers. Namely, we define the effective free energy of the quantum problem as

$$F = -\Re \ln A(x, y), \tag{15}$$

where A is the electron amplitude at the site (x, y), propagating in x-direction. This free energy describes the decay of the wave function. We compute the amplitude A by simulating electron propagation and check the scaling properties of its real part fluctuations in the y-direction and the universality of the distribution function.

We determine the amplitude A from the solution of the lattice recursive equation

$$A_{i,j} = \frac{g}{\epsilon_{ij}} \left[A_{i-1,j+1} + A_{i-1,j} + A_{i-1,j-1} \right], \tag{16}$$

where ϵ_{ij} are random independent variables defined on each lattice site and g is the parameter that determines the average decay of the amplitude (inverse localization length). Below, we discuss different distribution functions of ϵ_{ij} appropriate for different physical systems.

Physically, the model in (16) describes the motion of electrons on the lattice shown in Fig. 3. The site with the energy $\epsilon_{ij} = \langle \epsilon \rangle$ can be identified with the ideal lattice, the rest with impurities. If the energy ϵ_{ij} is distributed in a narrow interval around its average, evolution (16) becomes equivalent to (14) in the continuum limit. As discussed in Sec. 2.1, the physically most natural choices of the distribution function of ϵ are uniform $P(\epsilon) = \theta(\epsilon)$, linear $P(\epsilon) = 2\epsilon$, and their analogs for the negative scattering amplitudes, $P(\epsilon) = 1/2$ and $P(\epsilon) = |\epsilon|$. In all cases, we assume that the distribution is cut-off by ϵ_0 at large ϵ: $P(|\epsilon| > \epsilon_{max}) = 0$. The choice of ϵ_{max} determines the average decay rate

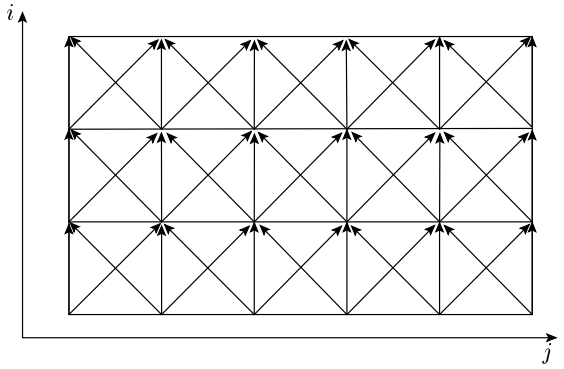

Fig. 3. Schematics of the electron propagation described by Eq. (16). The computation of the localization length discussed in Sec. 2.2 involves simultaneous propagation of amplitudes in the vertical direction for many (typically, $L > 10^6$) steps. For the computation of the matrix elements in Sec. 3.2, the wave functions were assumed to be localized on two sites in the middle of the upper and lower rows at a distance L and then determined in the middle

of the electron amplitude that is mostly irrelevant; in the computations, we have set it to $\epsilon_{max} = 1$. We have also studied the gapped distribution $P(\epsilon) = 2$ for $1/2 < \epsilon < 1$, for which we expect to obtain the results similar to the one predicted by the exact solution. Finally, we studied the binary distribution

$$P(\epsilon) = (1 - X)\delta(\epsilon - 1) + X\delta(\epsilon - (\mu + 1)^{-1})$$

characterized by a parameter X and a negative scattering amplitude $\mu < 0$.

Some of our results are presented in Figs. 4 and 5. For all the studied distribution, we observe very good scaling, $\left\langle \Delta F^2 \right\rangle^{1/2} \propto L^{\gamma}$, with the respective exponents $\gamma = 0.28$, 0.345, 0.343 for gapped, linear, and uniform densities of states. These values are very close to the expected value $1/3$, especially for the linear and uniform densities of states. The data for the gapped density of states display a significant transient regime, and therefore the deviation of the exponent from the analytic result is not surprising. The presence of negative scattering amplitudes has small effect on these exponents; they become $\gamma = 0.31$, 0.33, 0.345, which are even closer to the expected values. Furthermore, the higher moments of the distribution function tend to the universal values expected for the Tracy–Widom distribution. These results are in agreement with papers [44, 45] that observed the Tracy–Widom distribution of conductances in two-dimensional models.

These data lead to the conclusion that the main results of the directed polymer problem, the scaling dependence of the free energy and the universality of the distribution function, remain valid for the problem of electron tunneling in disordered media.

2.3. The sign phase transition

As explained in Sec. 2.1, the sign of the magnetoresistance is related to the statistics of signs of the amplitudes $A_{if}(0)$ in the absence of the magnetic field. If the concentration of impurities with negative scattering amplitudes is large, the sign of $A_{if}(0)$ becomes completely random. If all impurities are characterized by positive scattering amplitudes $\mu_i > 0$, the sign of $A_{if}(0)$ is positive. We let P_+ and P_- denote the respective probabilities to find a positive or negative amplitude $A_{if}(0)$. The quantity $\Delta P = P_+ - P_-$ characterizes the sign order. As the concentration X of the impurities with negative scattering amplitudes increases, ΔP should change from 1 to 0. Generally, ΔP is scale-dependent and acquires its limit value as $|r_i - r_f| \to \infty$. There are two logical possibilities: either at large scales $\Delta P_{r\to\infty} = 0$ only for $X > X_c$ while $\Delta P_{r\to\infty} > 0$ for smaller $X < X_c$, or any nonzero $X > 0$ leads to $\Delta P_{r\to\infty} = 0$. The former implies that the change in the X-dependence of the sign statistics can be viewed as a phase transition. This possibility has been suggested in [24, 25, 27], while the alternative was argued for in [31–33].

We study the sign statistics in the lattice models defined by (16) in Sec. 2.2 and show that both the phase transition and crossover can be realized depending on the distribution of ϵ. We start with the simplest case of the binary distribution

$$P(\epsilon) = (1 - X)\delta(\epsilon - 1) + X\delta(\epsilon + \epsilon_0)$$

with small $X \ll 1$ and small $\epsilon_0 \ll 1$. This model describes the wave function propagation on the ideal lattice (sites with $\epsilon = 1$) that contains rare impurities characterized by a negative scattering amplitude $\mu \approx -1/2\epsilon_0$, $|\mu| \gg 1$. The large value of $|\mu|$ allows a continuous description of the tunneling amplitude. The size of the region where the tunneling amplitude $A_{if}(0) < 0$ is negative can be found by noticing that the wave function

$$\Psi(x, y) = \exp\left(-\frac{x}{\xi}\right) + \frac{\mu}{(x^2+y^2)^{1/4}} \exp\left(-\frac{\sqrt{x^2+y^2}}{\xi}\right)$$

changes its sign in the egg-shaped region in the wake of the impurity given by

$$y^2(x) = x\xi \ln\left(\mu^2/x\right), \quad 0 < x < \mu^2.$$

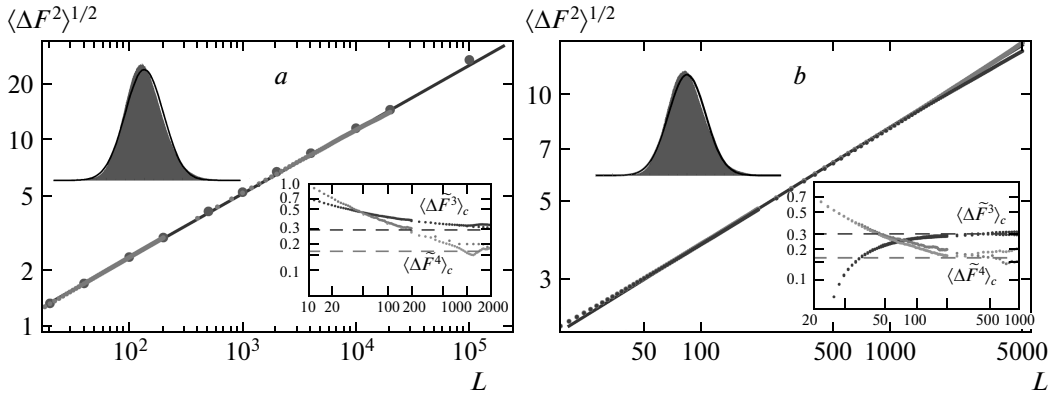

Fig. 4. Scaling dependence of fluctuations of the electron wave function decay, $\Delta F = \langle F \rangle - F$, where F is defined by (15). The quantity F is equivalent to the free energy of the directed polymer problem. a — the results for the linear density of states with $P(\epsilon < 0) = 0$, and b — the same results for the equally probable positive and negative scattering amplitudes. The upper insets show the distribution function of ΔF and its fit to the Gaussian, compared to which the distribution is slightly skewed as expected for the Tracy–Widom distribution. The lower insets show the evolution of the normalized higher moments of the distribution function that tends to the universal values expected for the Tracy–Widom distribution (shown as dashed horizontal lines). The numerical results were obtained by simulating evolution (16) on systems of sizes $N = 10^6$, 10^7, $5 \cdot 10^7$, as indicated by points of different size and colors. The straight line corresponds to the exponent $\gamma = 0.345$ (a), 0.33 (b). The convergence to the scaling form of the free energy fluctuations occurs relatively fast, while higher moments of the distribution function require enormous statistics, especially at large L, as is indicated by the deviation of curves representing the fourth moment for $N = 10^7$ and $N = 5 \cdot 10^7$

The area of this region is

$$S(\mu) = \frac{2}{3}\sqrt{\frac{2\pi}{3}}|\mu|^3\xi^{1/2}.$$

A small concentration $XS \ll 1$ of such impurities leads to independent lakes of negative signs shown in Fig. 6. In this situation, $\Delta P > 0$.

As the concentration X increases, different lakes start to overlap and form a state with random sign of the amplitudes. The transition between these two phases occurs at $X = X_c \sim S^{-1} \propto |\mu|^{-3}$. The dependence $P_-(X)$ is expected to have a general form characteristic of a phase transition, sketched in Fig. 7*a*. These qualitative arguments ignore the contributions from impurities located close to each other, which should not be relevant in the limit $X \to 0$.

The numerical simulations show that the transition also survives for not very large values of the scattering amplitudes. In particular, this transition has been observed for the binary distribution functions with $\epsilon_0 = 1$. Figure 7 represents the results of our numerical simulations for this case. As we can see, the behavior of ΔP as a function of the distance changes qualitatively as X increases beyond $X_c \approx 0.032$. For smaller concentrations x, the probability difference ΔP saturates at nonzero values, while for larger concentrations, it approaches 0. The scales needed to observe this change in the behavior are generally very long. We believe that this is the reason that prevented unambiguously establishing the existence of the transition in early numerical simulations. We note that the scales are further enlarged near $X_c \approx 0.032$, as is expected at a phase transition.

We have also checked that the phase transition between the sign-ordered and sign-disordered phases survives for a gapped distribution of ϵ defined in Sec. 2.2. The numerical data look very similar to those shown in Fig. 7, the value of X_c in this model is $X_c \approx 0.02$.

The existence of the sign phase transition has been questioned in paper [33], which used the mapping to the directed polymer problem. The essence of the argument is that the free energy of directed polymers leading to a given site are dominated by a single path, and hence just a single impurity along this path suffices to change the sign of the amplitude. At a small concentration of negative scatterings, one concludes that the amplitude should become completely random at the scale $L \propto 1/X$. This argument, however, does not take the contribution from subdominant paths into account, which may eventually restore the sign of the amplitude at large scales, as is indicated by numerical data for the gapped density of states (see Sec. 2.2).

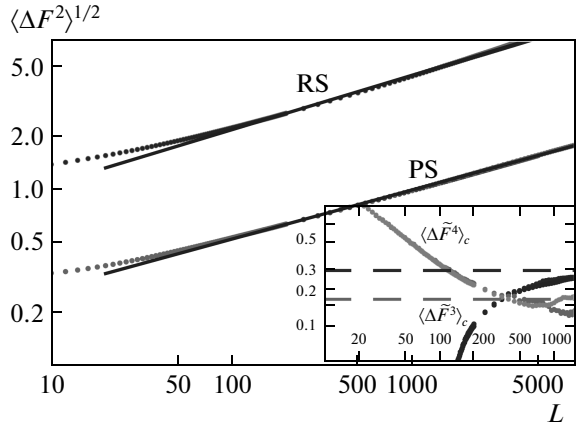

Fig. 5. Scaling dependence of fluctuations of the electron wave function decay $\Delta F = \langle F \rangle - F$ obtained from the numerical solution of evolution (16) with a gapped density of states. The lower data set (denoted by PS) corresponds to the positive scattering amplitudes, and the upper data set (denoted by RS), to the completely random amplitudes with equal probability of signs. The data were fitted with the scaling dependences with the exponent $\gamma = 0.28$ for positive scatterers and $\gamma = 0.31$ for random signs. The results were obtained for the systems of size $N = 10^7$, $5 \cdot 10^7$. Higher moments tend to the universal values of the Tracy–Widon distribution as shown in the inset, which gives the data for random-sign scatterers

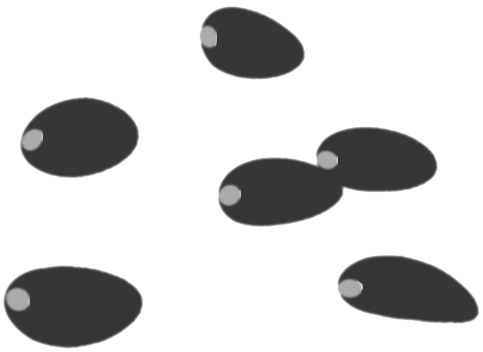

Fig. 6. Qualitative picture of lakes of negative amplitude signs formed in the wake of an impurity (shown as a small gray circle) characterized by a negative scattering amplitude

We now show that for a gapless density of states (3) with $\beta < 2$ and for any nonzero concentration of negative scatterers, the sign of the amplitude A becomes completely random at large scales. Indeed, in this case, the total area of negative lakes is

$$S_{tot} \sim X \int d\epsilon \nu(\epsilon) S[\mu(\epsilon)],$$

where $S[\mu] \propto \mu^3 \propto \varepsilon^{-3}$. Hence, S_{tot} diverges for all densities of states $\nu(\epsilon) \sim \varepsilon^\beta$ with $\beta \leq 2$. For example, this is the case for the Coulomb gap, where $\nu(\epsilon) \propto \varepsilon$.

We have checked this conclusion numerically for the linear density of states and we have indeed observed that even a very small $X \sim 10^{-4}$ leads to a random sign of the amplitude at very large scales. Our data are shown in Fig. 8. As expected, the scale at which the sign becomes random grows quickly with the decrease in X.

3. MAGNETORESISTANCE IN THE HOPPING REGIME

3.1. Magnetic field dependence of the localization length

We now turn to the discussion of magnetoresistance in the variable-hopping regime. We begin by summarizing the results of numerical simulations for recursive equation (16) that was modified to include the phases $\phi_j = Bj$ induced by magnetic field

$$A_{i,j}(B) = \frac{1}{\epsilon_{ij}}[A_{i-1,j-1}e^{i\phi_{j-1/2}} + A_{i-1,j}e^{i\phi_{j-1/2}} + A_{i-1,j+1}e^{i\phi_{j+1/2}}]. \quad (17)$$

Then we give the qualitative explanation of the results based on the mapping of hopping to the directed polymers. The dimensionless magnetic field B in this equation and in the discussion below is given by the flux of the physical magnetic field B_{phys} through the elementary square plaquette of the lattice: $B = B_{phys}a^2/\Phi_0$, where a is the lattice constant and $\Phi_0 = hc/e$ is the flux quantum.

Our main result is that at large $r_{hop} > L_B$ (which holds at low temperatures), both positive and negative magnetoresistances are described by corrections to the localization length:

$$g(B) = \frac{\Delta\xi(B)}{\xi(0)} = \pm C_\pm \left(\frac{B\xi^2}{\Phi_0}\right)^\alpha. \quad (18)$$

This scaling law is characterized by the universal exponent $\alpha \approx 4/5$ and nonuniversal numerical coefficients $C_\pm$. The latter depend on the distribution of ε_{ij}, e. g., $C_+ \approx 2.6$ for the gapped and $C_+ \approx 0.9$ for linear density of states. Here, we define the localization length as the limit $\xi = \lim_{r_{ij}\to\infty} \ln A_{ij}(B)/r_{ij}$. The positive sign (+) in (18) corresponds to the case where the system is in the sign-disordered phase and the negative

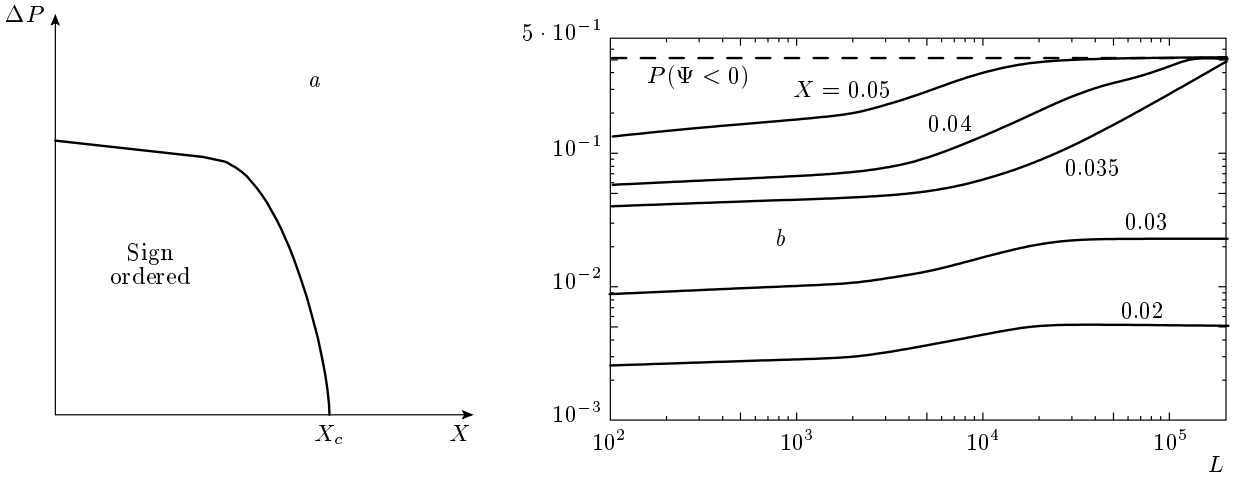

Fig. 7. a — Qualitative picture of the phase transition described by the order parameter $\Delta P(X)$ that occurs at $X_c \approx 0.032$ for the the binary distribution described in the text. b — Scale dependence of the probability of the negative amplitude, showing the transition around $X_c \approx 0.032$

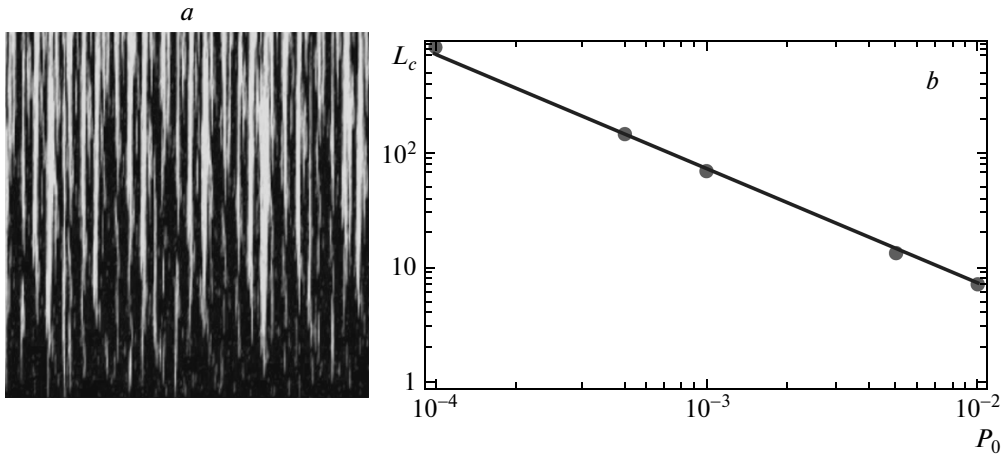

Fig. 8. a) The map of the amplitude sign resulting from the wave function evolution in the vertical direction for the linear density of states. The wave function has all positive signs (shown in black) at the beginning of the evolution (bottom). As the evolution goes upward, the presence of a small concentration $X = 10^{-4}$ of negative scattering amplitudes results in a larger and larger regions of negative signs (white regions) until the whole amplitude sign becomes completely random at the top. b) The length scale $L(X)$ at which the sign becomes random as a function of the concentration X. Here, we define $L(X)$ as the length at which $\Delta P = 0.25$. The data fit well with the dependence $L \propto 1/X$, in agreement with the theoretical expectations based on the directed polymer mapping

sign $(-)$ corresponds to the sign-ordered phase. The universal regime (18) is achieved at low fields. We note that while the value of $\xi(B)$ is mathematically defined for any magnetic field, its applicability to the hopping problem requires that $r_{hop} > l_B$.

At intermediate fields, a slightly different power law

$$g(B) = \frac{\Delta\xi(B)}{\xi(0)} = \pm D_{\pm} \left(\frac{B\xi^2}{\Phi_0} \right)^{\alpha'} \qquad (19)$$

if often observed with a different exponent and prefactors, $\alpha' \approx 0.5,\ 0.6,\ 0.64$ for the scattering of random signs with gapped, linear, and uniform densities of states respectively. For these densities of states the prefactors are $D_+ \approx 0.11,\ 0.22,\ 0.30$. The value of D_+ for the gapped density of states is in agreement with the previous numerical simulations in [26, 28]. We note that the value of D_+ for the uniform density of states is roughly three times larger than for the gapped one.

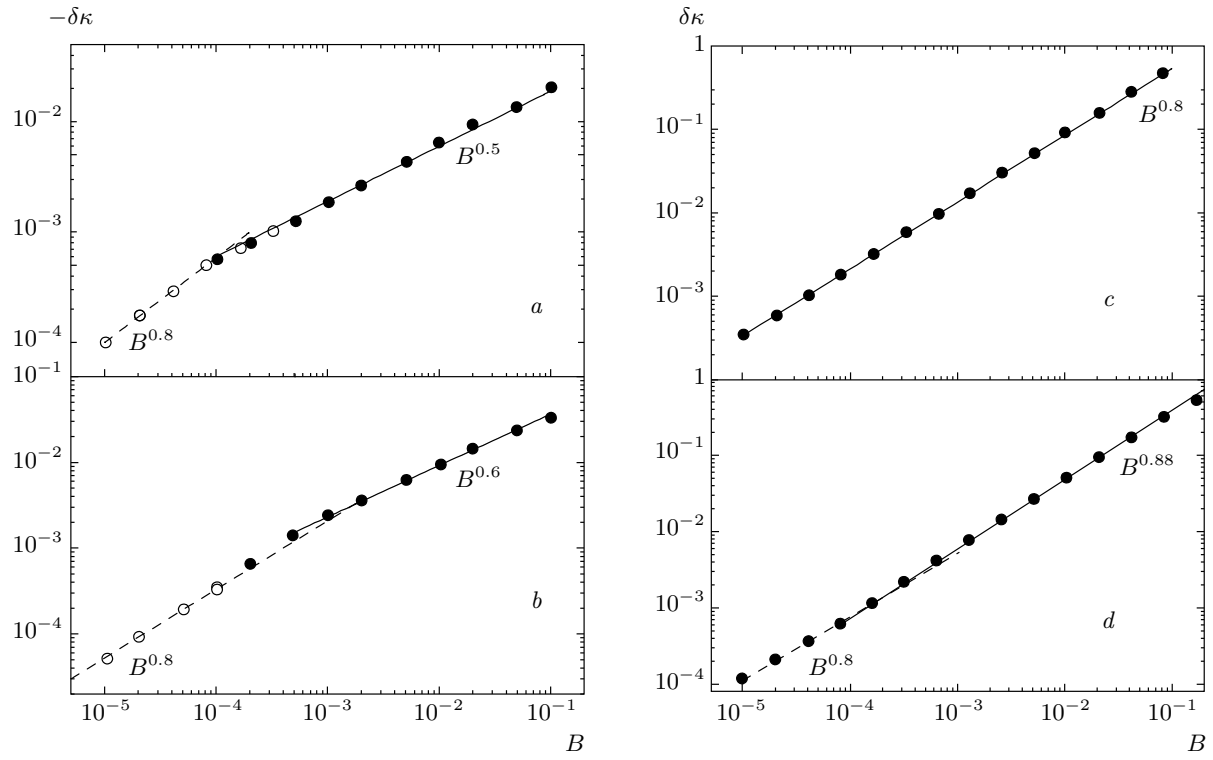

Fig. 9. Change in the inverse correlation length $\delta\kappa = \delta(1/\xi)$ induced by the magnetic field. a,c correspond to the gapped density of states and b,d — to linear density of states. a,b correspond to random scattering amplitude signs and c,d — to positive scattering. The absolute values of the inverse correlation length at $B = 0$ in these cases are $\xi_0^{-1} = 1.85,\ 1.42$ for gapped and linear densities of states, and $X = 0.5$ and $\xi_0^{-1} = 1.31,\ 0.95$ for uniform and linear density of states for positive scattering ($X = 0$). The results for the constant density of states (not shown) are very similar to the ones for the linear density of states shown in b,d: they display a large domain of the intermediate regime of power-law behavior with the respective exponents 0.6 and 0.9 for $X = 0.5$ and $X = 0$

This makes it possible to observe large negative magnetoresistance experimentally, as we discuss in Sec. 5. These statements are illustrated in Fig. 9. The scaling dependence with the exponent $\alpha' \approx 0.6$ was observed previously in a number of works [28, 32], in which insufficient system sizes prevented the observation of the asymptotic behavior.

We now give qualitative arguments that reproduce the observed scaling behavior of the change in the localization length explained above.

As we have shown in Sec. 2.2, the problem of electron tunneling belongs to the same universality class as the problem of directed polymers. In particular, the typical tunneling action varies from one path to another by the amount that scales as $\Delta F \propto L^{1/3}$. This means that the tunneling from point i to f is dominated by a narrow bundle of paths, as shown in Fig. 10. The width of this bundle does not increase with the length of the path, and hence the magnetic field has very little effect on the tunneling in this approximation. Another bundle of paths that differs from the dominant one at a scale L has the action that is typically larger than that of the dominant path by $\Delta F \propto L^{1/3}$, and therefore its amplitude is exponentially suppressed by $\exp\left[-c(L/a)^{1/3}\right]$, where a is the mean free path of the electron (lattice spacing in the case of numerical simulations). This leads to an exponentially small effect of the magnetic field. However, because the difference of the actions between two paths is a random variable itself, with probability $p \propto L^{-1/3}$ two actions differ only by the amount of the order of unity. If all scattering amplitudes are positive, the change in the interference caused by the magnetic field decreases the total amplitude by the factor of the order of unity, if the flux through the loop formed by these two paths is of the order of the flux quantum. Because the transverse direction scales as $Y \sim a(L/a)^{2/3}$, the interference becomes relevant at scales $\sim L$:

$$BL^{5/3}a^{1/3} \sim \Phi_0 \tag{20}$$

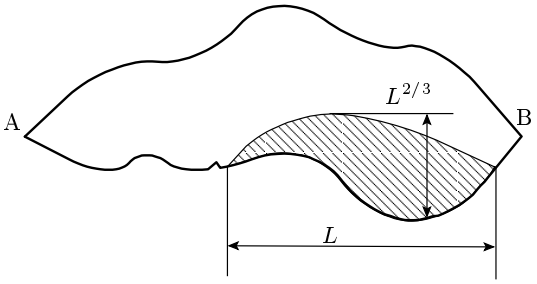

Fig. 10. Directed polymer picture

with probability $p \sim (L/a)^{-1/3}$. The resulting decrease of the wave function implies that the typical inverse localization length increases by

$$\delta\xi^{-1} \sim a^{1/3}/L^{4/3} \sim (B/\Phi_0)^{4/5} a^{3/5}.$$

Repeating the same arguments for the amplitudes of the random signs and using the fact that the signs of two paths that contribute to the interference are random (cf. the discussion after Eq. (11)), we obtain the same dependence on magnetic field but with the opposite sign: the inverse localization length is decreased by the magnetic field.

All these conclusions are valid in the limit of long scales, where $\Delta F \gg 1$. In the intermediate regime, with $\Delta F \lesssim 1$, the probability that two paths interfere is of the order of unity, resulting in the scaling dependence of $\delta\xi^{-1}$ on the field with the exponent $\alpha' = 3/5$. Looking at the numerical results for the scaling dependence of ΔF shown in Fig. 4, we see that it remains of the order of unity for $L \lesssim 10^2$, which translates into the field $B \gtrsim 10^{-3}$, in rough agreement with the numerical results shown in Fig. 9.

The behavior of the correlation length is given by simple scaling equations (18) and (19) only in the limit of completely random and positive amplitude signs. In the case of a small concentration of negative scatterings, a more complicated behavior is expected. Large fields affect the amplitude at short scales. At these scales, the rare negative scatterings have small effect on the amplitude sign, and hence at large fields the inverse localization length is increased by the field, similarly to the case of positive scattering amplitudes. By contrast, at large scales relevant for small fields, the amplitude sign becomes completely random, and therefore a negative correction to $\delta\xi^{-1}$ is expected at small fields, similarly to the fully random sign case. As the field is increased, the sign of the correction should change. Exactly this qualitative behavior is shown by numerical simulations of model (17) with a small concentration of scatterers with negative amplitudes. Our

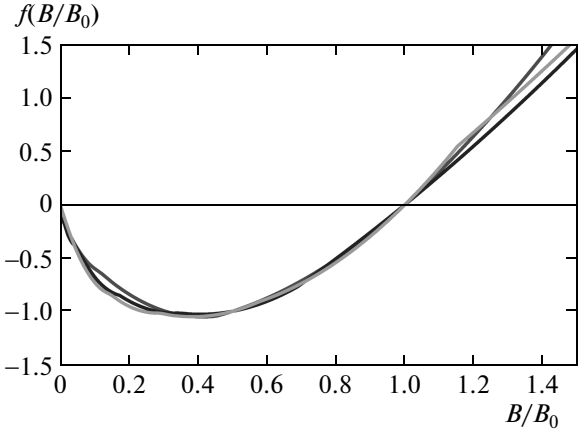

Fig. 11. Universal behavior of the increment of the inverse localization length as a function of the field for a small concentration of negative ϵ_{ij} and the linear density of states. Different curves show $\delta\xi^{-1}$ for different concentrations $X = 0.02,\ 0.08,\ 0.16$ rescaled in both vertical and horizontal directions: $\delta\xi^{-1} = \delta\xi_0^{-1}\chi(B/B_0)$. The characteristic value of the field scales with X as $B_0 \propto X^\beta$ with $\beta \approx 2.8$. Very small values of the field imply that the negative correction of $\delta\xi^{-1}$ wins over the positive one only when signs are completely randomized; even a small correlation between the signs of the amplitude suffices to result in a positive correction

results shown in Fig. 11 display universal behavior of $\delta\xi^{-1}(B/B_0)$. The characteristic field B_0 scales, as expected, with the concentration X: $B_0 \propto X^\beta$, but the exponent $\beta \approx 2.8$ is sufficiently larger than the one expected from the scaling behavior of $L(x) \propto 1/x$ obtained in Sec. 2.3: $\beta_{expected} \approx 1.6$. We do not have a satisfactory explanation of this discrepancy. We only note that very small values of B_0 found numerically imply that even a small amount of sign correlations is sufficient to result in the positive $\delta\xi^{-1}$. This is not so surprising because the positive increment of $\delta\xi^{-1}$, although given by the same scaling dependence, is an order of magnitude larger than the negative one (cf. Fig. 9*a*,*b* and Fig. 9*c*,*d*).

The scaling dependence in (18) is nonanalytic in B, and should therefore dominate over other sources of corrections to the localization radius as $B \to 0$. In the electron hopping problem, the largest scale r_{hop} for the coherent electron tunneling is set by temperature (1). The nonanalytic behavior predicted by (18) occurs if the scale L given by (20) is less than $r_{hop}(T)$:

$$\left(\frac{\Phi_0}{B}\right)^{3/5} a^{1/5} < \xi \left(\frac{T_0}{T}\right)^{\zeta}.$$

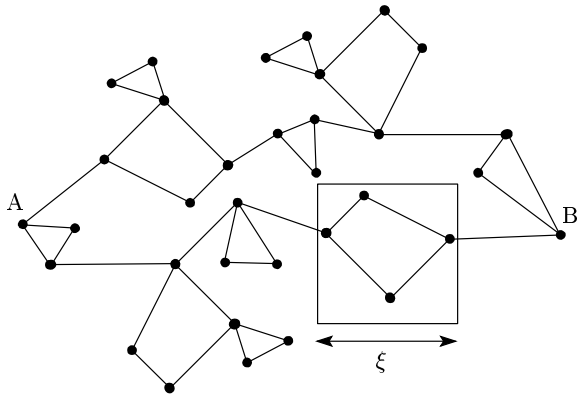

Fig. 12. Quantitative picture of tunneling paths in the vicinity of the metal–insulator transition in the case where $\xi > a_B$. The path may contain return loops at short scales (of the order of ξ), but the electron moves only in one direction at longer scales. We expect that the problem is mapped onto directed polymers at scales larger than ξ, and hence small magnetic fields $B\xi^2 \lesssim \Phi_0$ are expected to have the same effect on the resistivity as in the strongly localized regime

In the discussion of the hopping transport, we have assumed the strongly localized regime in which the electron wave function is localized at scales of the order of the Bohr radius a_B of a single impurity. However, all our qualitative conclusions should also hold when the localization length is larger, $\xi > a_B$. In this case, the electrons tunnel from one area to another as is shown in Fig. 12. The loops of the tunneling paths are allowed inside individual areas, but not between them. In this regime, we expect to observe large nonanalytic dependence of the localization length on the magnetic field given by (18) and (19) at low fields $B\xi^2 \lesssim \Phi_0$. These universal corrections add to the effect of the magnetic field coming from the scales shorter than ξ, which can be found from the renormalization group approach. These corrections are of the order of $\delta\xi/\xi \sim (B\xi^2/\Phi_0)^2$ and are therefore negligible compared to the effects in (18) and (19) coming from the longer scales at low fields. However, they can contribute significantly to the total variation of the magnetoresistance at large fields.

3.2. Magnetoresistance in the variable-range hopping regime

The results (18) and (19) for the $\xi(B)$ dependence can be converted into magnetoresistance if the induced change of the localization length is small, $\delta\xi \ll \xi$, but the resulting change in the hopping amplitude is exponentially large, leading to resistance variations $\ln(\rho(0)/\rho(B)) \gg 1$. In this case, we can neglect other contributions to the variation of the hopping probability (which we discuss below), and the magnetoresistance is given by

$$\ln\frac{\rho(B)}{\rho(0)} \approx \left[2\zeta\left(\frac{T_0}{T}\right)^{\zeta}\right]\frac{\delta\xi}{\xi}. \qquad (21)$$

Combined with the $\xi(B)$ dependence discussed in Sec. 3.1, this equation gives the magnetoresistance at moderate fields, such that $B\xi^2 \lesssim \Phi_0$ but $\ln(\rho(0)/\rho(B)) \gg 1$.

At large magnetic fields $B\xi^2 \gtrsim \Phi_0$, Eq. (21) remains valid, but the localization length dependence on the magnetic field is due to short scales and is nonuniversal. For a granular metal, the localization length is roughly equal to the grain size r_0; because the magnetic field has no effect at scales shorter than r_0, the $\delta\xi(B)$ dependence saturates at $B\xi^2 \lesssim \Phi_0$. By contrast, in the case of a weakly disordered noninteracting $2D$ metal with $kl_{tr}>1$, one expects [7] a strong dependence on the magnetic field. Indeed, in this case, the localization length is exponentially large $\xi(0) \sim l_{tr}\exp(k_F l_{tr})$ in the absence of the magnetic field, with l_{tr} being electron mean free path. The conventional renormalization group analysis [7] gives $\delta\xi(B)/\xi(0) \sim (B\xi^2/\Phi_0)^2$ at $B\xi^2 < \Phi_0$, and corrections of the order of unity are therefore expected at $B\xi^2 \approx \Phi_0$. At larger fields ($Bl_{tr}^2 \sim \Phi_0$), the localization length increases exponentially to $\xi(B) \sim l_{tr}\exp(k_F l_{tr})^2$. At even larger fields, the appearance of the quantum Hall regime and a pseudometallic behavior are expected [13]. The presence of electron–electron interaction can lead to an even greater variety in the localization length dependence on the magnetic field at high fields.

The computation of the $\xi(B)$ dependence in Sec. 3.1 translates into the predictions for magnetoresistance (21) only in the asymptotic regime of large magnetic fields at which $\ln(\rho(0)/\rho(B)) \gg 1$. There are at least two reasons why it is important to study the magnetoresistance in the opposite limit of low magnetic field.

First, because it is difficult to measure large resistances, the parameter $r/\xi \lesssim 15$ cannot be very large, and therefore the condition $\ln(\rho(0)/\rho(B)) \gg 1$ is satisfied only in a limited range of fields. As we show below, the power-law dependence of $\ln(\rho(0)/\rho(B))$ extends somewhat in the regime if $\ln(\rho(0)/\rho(B))) \lesssim 1$, which makes the observation of this dependence more realistic.

Second, many experimental data show that the magnetoresistance often changes sign in small fields. As we discuss in more detail below, this sign change agrees with the theoretical expectations. For instance, if the

scattering amplitudes are mostly positive ($P_- \ll 1$), the localization length at large fields becomes shorter (see Sec. 2.3) and magnetoresistance is positive. But it may change its sign and become negative at small fields. This change in the sign of the magnetoresistance can be due to the change in the sign of the correction to the localization length discussed in Sec. 2.3 or to another effect at short scales that we discuss below. Generally, the theoretical predictions in this regime are less universal.

At small magnetic fields, the accuracy of the approximation $M_{ij} \sim A_{ij}$ becomes insufficient because it overestimates the contributions to hopping rate (4) from the impurity configurations in which the partial amplitudes $A_\Gamma(0)$ cancel each other in the absence of the magnetic field, whence $A_{if}(0) \approx 0$. For these configurations, a small magnetic field changes $\ln A_{if}$ dramatically. For a finite probability density of $A_{ij}(0) = 0$, the magnetic field dependence of $\overline{\ln A(B)}$ becomes a nonanalytic function of B: $\overline{\ln[A(B)/A(0)]} \propto |B|$ [24, 25]. Similarly to the qualitative discussion of the $\xi(B)$ dependence in Sec. 3.1, this nonanalyticity can be demonstrated in the case where the propagation amplitude is due to the interference between just two paths, $A_{if} = A_1 + A_2 \approx 0$ with random A_1 and A_2. In this model case, the typical amplitude in a magnetic field becomes

$$\overline{\ln\left|\frac{A(B)}{A(0)}\right|} = \int dA_1 dA_2 \ln\left|A_1 - A_2 e^{i\phi}\right| \sim |\phi|, \quad (22)$$

where $\phi \propto B$ is the phase difference induced by the magnetic field. Here and below, we let the bar denote the averaging over the impurity configurations. Because the probability density of $A_{ij}(0) = 0$ is finite at any concentration of scatterers with $\mu_i < 0$, the typical amplitude always increases at small fields. But this does not always translate into negative magnetoresistance.

The crucial difference between the amplitude A_{ij} and hopping rate (4) is that the latter is the sum of the positive rates due to phonons with different q directions. As a result, the probability density to find $W_{if} = 0$ is zero, and the magnetorsistance is proportional to B^2 at small B.

To find the values of the crossover fields, we note that in the limit of low temperatures at which $qr_{ij} \ll 1$, the exponential in (5) can be approximated by the first nonzero term:

$$M_{ij}(\mathbf{q}) \sim \int d\mathbf{r} \psi_i^\dagger(\mathbf{r}) \psi_j(\mathbf{r}) \mathbf{q}\cdot\mathbf{r}. \quad (23)$$

The main contribution to the matrix element M_{ij} comes from the components of the phonon wave vector $\mathbf{q}$ that is parallel to $\mathbf{r}_{ij}$. In the leading approximation, we can neglect the contributions from the phonons with momenta in other directions. In this approximation, the hopping probability (4) is controlled by the matrix element $M_{ij}(q\hat{r}_{ij})$ $\hat{r}_{ij} = \mathbf{r}_{ij}/r_{ij}$. This matrix element has the same statistical properties as the amplitude A_{if}, and therefore the reasoning resulting in (22) applies, whence

$$\overline{\ln|M(B,\mathbf{q})/M(0,\mathbf{q})|} \sim |B|.$$

The subleading processes in which hopping (4) is due to phonons with momenta perpendicular to $\mathbf{r}_{ij}$ cut off the nonanalytic behavior of $\overline{\ln W(B)}$ at very small fields.

Combining this result with the effect of the $\xi(B)$ dependence discussed in Sec. 3.1 that occurs at large scales at which the flux through the typical loop is larger than the flux quantum, $Br^{5/3}\xi^{1/3} > \Phi_0$, we obtain three regimes of the $\overline{\ln M(B)}$ dependence for $B\xi^2 < \Phi_0$:

$$\ln\frac{\rho(0)}{\rho(B)} = \overline{\ln\frac{W_{if}(B)}{W_{if}(0)}} \sim \sim \begin{cases} (B/B_0)^\alpha \gtrsim 1, & B > B_0, \\ |B|/B_0 \lesssim 1, & B_0 > B > B_*, \\ B^2/B_* B_0 \ll 1, & B < B_*, \end{cases} \quad (24)$$

where $B_0 = \Phi_0/r^{5/3}\xi^{1/3}$. As we saw in Sec. 3.1, the transverse deviations of the typical path scale as $r_\perp \sim r^{2/3}\xi^{1/3}$. This allows us to estimate the contribution to the average in (4) from phonons with $q \perp r$: $W_\perp \sim (\xi/r)^{2/3} W$. Repeating the arguments that led to (22), we obtain

$$\overline{\ln\frac{W(B)}{W(0)}} = \int dW_\parallel \ln\left[W_\parallel + W_{typ}\phi^2 + W_\perp\right], \quad (25)$$

which results in the dependence (25) with $B_* = \Phi_0/r^2$.

The qualitative estimates show that while the regime of a nonanalytic dependence is relatively wide ($B_0 < B < \Phi_0/r^2$), the regime of the linear dependence is narrow. We note that the estimates of B_* and B_0 neglect the numerical coefficients that might be important.

The discussion above and the result in (24) assumed that the system is deep in the sign-disordered phase, in which signs of all amplitudes are completely random. If the scattering amplitudes are mostly positive, $P_- \ll 1$, the signs of the amplitudes become random only at large scales. This implies that the system can be in

the sign-ordered phase at characteristic scales set by the magnetic field. In this case, the magnetoresistance at largest fields is positive in contrast to (24), while at small B it is quadratic in B, and can therefore be both positive and negative depending on the value of $P_- \ll 1$.

To verify the validity of (25) for realistic parameters, we have performed the numerical computation of the matrix elements. We did not attempt a full computation of the matrix element and its averaging over the distribution of r_{ij} that characterize the percolating cluster. Instead, we computed the matrix element for the characteristic r_{ij} and averaged over different direction of q. Because the results do not change qualitatively when r is increased by a factor of 2, we believe that they faithfully reproduce the dependence of the magnetoresistance:

$$\ln \frac{\rho(0)}{\rho(B)} = \ln \frac{\overline{\langle M^2(B)\rangle_q}}{\overline{\langle M^2(0)\rangle_q}}, \qquad (26)$$

where the angular brackets denote averaging of the directions of $\mathbf{q}$. The result of our numerical simulations for the uniform density of states $P(\epsilon) = (1/2)\theta(1-|\epsilon|)$ is shown in Fig. 13 for two typical distances: $r/\xi \approx 8$ and $r/\xi \approx 6$. In both cases, we observe a large regime of the pseudo-universal behavior $\ln(\rho(0)/\rho(B)) \sim B^\alpha$ with $\alpha \approx 0.5$, which is due to the nonuniversal corrections to localization length (19). At larger $r/\xi \gtrsim 8$, we observe the gradual appearance of the transient linear dependence in the magnetic field, in agreement with the expectations from (25). Figure 14 shows the expected magnetoconductance at different typical values of r/ξ converted into expected values of the resistances.

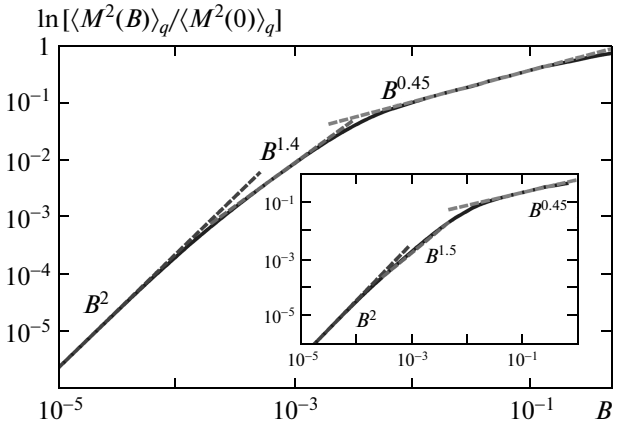

Fig. 13. Phonon matrix element as a function of the magnetic field at long and moderate scales. The main panel shows the field dependence of the matrix element for relatively long hops corresponding to $r/\xi \approx 8.0$. We observes a very significant (two decades) regime of the pseudo-universal scaling dependence associated with the localization length dependence in (19). At shorter scales (corresponding to $r/\xi \approx 6$ shown in the inset), the scaling regime shrinks. In both cases, the regime of the analytic dependence (B^2) is limited to very small fields

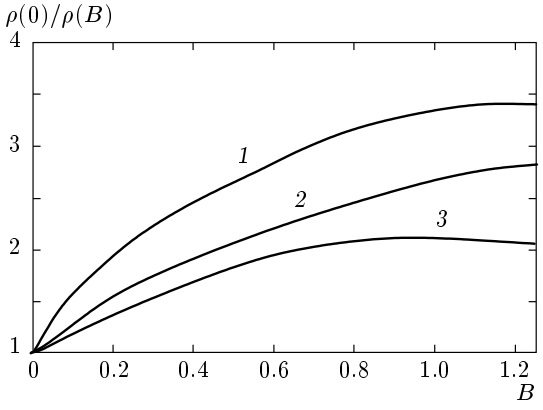

Fig. 14. Magnetoconductance as a function of the magnetic field for different values of the matrix element at zero field corresponding to $R_\square/R_Q \approx 5 \cdot 10^5$ (*1*), 10^4 (*2*), 10^3 (*3*). For small matrix elements (large resistances), the behavior at low fields can be approximated by a power law $\sigma(B)/\sigma(0) \approx B^a$ with $a \approx 0.5 - 0.6$. The regime of very small magnetic fields is hardly observable on the linear scale of the plot even for smallest resistances

3.3. Beyond the single particle model

So far in our discussion we have ignored the many-body effects due to electron–electron interaction. Generally, one expects that electron correlations play a much bigger role in the hopping regime than in the metallic regime. In this subsection, we briefly discuss their role and the conditions under which the single-particle results obtained above are valid.

At low temperatures, the electron sites with $\epsilon_\alpha < 0$ (and $\mu_\alpha < 0$) are occupied by electrons, while the sites with $\epsilon_\alpha > 0$ are empty. Tunneling between initial and final states can be viewed as a virtual process in which the electron hops through the intermediate localized states. Depending on the ratio between the electron–electron interaction and the density of states

at the Fermi energy in the impurity band, these localized states can be singly and doubly occupied. The spins in the singly occupied states interact via the exchange interaction J. Although the detailed theory of disordered electron systems does not exit, three obvious limit cases are clearly possible. In the first case, the interaction between electrons is large, the majority of sites are singly occupied, and the resulting spin system might form an $S = 1/2$ spin glass at low temperatures and a paramagnet at high temperatures. The low-temperature spin glass state breaks the time-reversal symmetry; it might be collinear or isotropic depending on the anisotropy of the exchange couplings. Although logically possible, neither collinear nor isotropic states were observed experimentally, probably because quantum spin fluctuations are too large for spin 1/2. The alternative (second case) is that each spin forms a singlet with another spin to which it is coupled by the strongest interaction [46]. This state does not break the time-reversal symmetry. Finally, in the limit of small interaction, the majority of states are doubly occupied (third case). Both the second and third cases are characterized by zero average spin on each site.

In all cases, the segments of the tunneling path where electrons travel through occupied sites can be viewed as a tunneling of a hole moving backwards through occupied states, as is schematically shown in Fig. 2. In the interacting system, this process can lead to the creation of many-body excitations in the final state that destroy the coherence between hopping amplitudes A_Γ along different paths Γ. When this does not happen, the tunneling can be described by Eq. (7) with renormalized hopping amplitudes and energies ϵ_a.

We now discuss the tunneling interference in different electron states in more detail. We start with a state in which all sites are singly occupied. At high temperatures, the resulting spins form a paramagnet, and hence the final spin states formed after the charge transport along different paths Γ are generally different and do not coincide with the initial state. In this state, the corresponding amplitudes A_Γ do not interfere. In this situation, no orbital effects of the magnetic field on the charge transport are expected. Application of the magnetic field can polarize the spin system, restoring the path interference. Thus, in this case, we expect that the polarization of the spin system by the in-plane field results in a state characterized by a large negative magnetoresistance with respect to the field perpendicular to the plane, while application of a small perpendicular field in the absence of an in-plane one gives small or no negative magnetoresistance. A large out-of-plane field (in the absence of the in-plane field) has two effects: it might polarize the spin system and cause orbital effects. Thus, we expect a complicated behavior as a function of the out-of-plane field.

At low temperatures, the spins may freeze in a spin glass state or form a spin liquid. If the spins freeze in the collinear spin glass state, the final states corresponding to two paths mostly coincide and the interference reappears. In this situation, the electron hopping amplitude can be described by essentially the same equation (7). Thus, we expect the same orbital effect of the magnetic field as discussed in Sec. 3.1.

The electron hopping becomes very different in the noncollinear spin glass because the electron amplitudes acquire a nontrivial phase factors due to spin noncollinearity, which can be described by complex scattering amplitudes μ_a. We expect that the magnetic field does not affect the interference in this case and does not lead to orbital magnetoresistance. However, the isotropic spin glass state is rather unlikely to be realized in physical two-dimensional and even three-dimensional glasses [47].

In contrast to the spin glass states, the spin singlets formed in the second and third cases do not break the time-reversal symmetry. Thus, the scattering amplitudes in these situations remain real as in the single-particle model. At low temperatures, the final states formed after charge motion should coincide, and hence the interference between different paths remains the same as it was in the one-particle model in Sec. 3.1.

We do not discuss the effect of the magnetic field on the spin configuration, which also affects the transport of charges. This discussion is beyond the scope of this paper devoted to the orbital effects. But we briefly mention possible scenarios in Sec. 5, where we discuss the experiment that indicates that these effects are important.

4. APPLICATION TO OTHER PHYSICAL SYSTEMS

The sign phase transition that appears for the binary distribution of scattering amplitudes discussed in Sec. 2.3 can be observed in very different physical systems. Here, we show that it affects the physics of random classical magnets at high temperatures. The simplest example is given by the Ising model on a cubic lattice

$$H = \sum_{i,j} J_{ij} s_i s_j, \tag{27}$$

where $s_i = \pm 1$ and the exchange interaction takes two values: $J_{ij} = J_0 > 0$ with probability $1 - X$ and $J_{ij} = -J_0$ with probability X.

At high temperatures, the susceptibility in this model is given by

$$\chi(\mathbf{r}_i, \mathbf{r}_f) = \langle s(\mathbf{r}_i) s(\mathbf{r}_f) \rangle = \\ = \sum_{\{s_0\}} s(\mathbf{r}_i) s(\mathbf{r}_f) \exp\left(-\frac{H}{T}\right), \quad (28)$$

which is a random quantity at large $r_{if} \gg 1$. To show the existence of the sign phase transition in this quantity, we notice that at $T \gg |J_{ij}|$, we can expand the exponent in (28) and take only directed paths between sites i and f into account. Summing over directed paths is equivalent to solving the recursion equation

$$\chi_{km} = \chi_{k-1m} J^{km}_{k-1m} + \chi_{,m-1} J^{km}_{km-1n}, \quad (29)$$

where indices "km" denote the site with coordinates k, m on the square lattice and J^{km}_{k-1m} denote the bond connecting two such sites. Recursion (29) is very similar to (16) with the binary distribution of ϵ_{ij}, and we can therefore expect that it shows the same sign transition as a function of the concentration X of negative bonds. The only difference between (29) and (16) is that the negative signs are associated with bonds in the former and with sites in the latter. This is similar to the difference between site and bond disorder in the percolation problem which is known to have very little effect. Thus, we expect that at $r \to \infty$, the distribution function of $\chi(r)$ exhibits the sign phase transition as a function of X. At high temperatures, the critical value X_c is T-independent. As the temperature decreases, the sign correlations increase, which can lead to the formation of the sign-ordered phase. This means that the transition from the spin-disordered to spin-ordered phase shifts to larger X at lower temperatures. Finally, at sufficiently low temperatures, the system might become a ferromagnet. At the transition point, susceptibility (28) decreases as a power of $|r_i - r_f|$ and the sign correlations are long-range whereas spin correlator decreases exponentially. Thus, the transition to the sign-ordered state occurs above the transition to a ferromagnet.

The staggered susceptibility is defined by $\tilde{\chi}(r) = (-1)^n \chi(r)$, where n is the number of steps in a direct path on a square lattice between the sites 0 and r. Obviously, it also exhibits a sign phase transition. Thus, at high temperatures, the sign-disordered phase is separated from the phases in which the sign of the susceptibility is positive or alternating. At sufficiently low temperatures, the system freezes into a magnetically ordered or a spin glass phase. The spin glass phase may be sign-ordered or sign-disordered, the former corresponds to the coexistence of ferromagnetic (or antiferromagnetic) and spin glass order parameters. These conclusions are summarized by the phase diagram shown in Fig. 15.

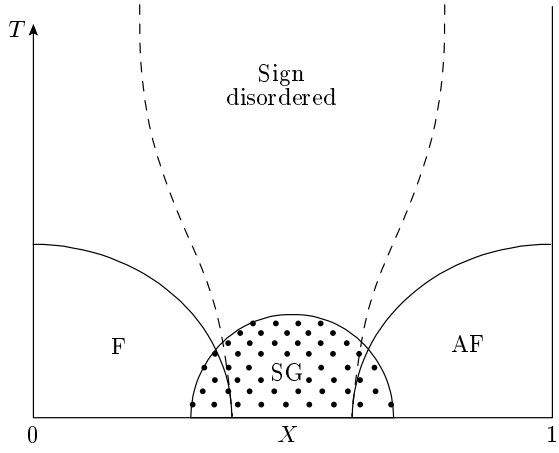

Fig. 15. Qualitative picture of the phase diagram of Ising spin glass. Dashed lines separate sign-ordered and sign-disordered phases at high temperatures. The spin glass phase (SG, dots) appears in dimension three and higher. In two dimensions, the spin system remains paramagnetic down to lowest temperatures in the absence of the ferromagnetic (F) (or antiferromagnetic (AF)) long-range order

5. REVIEW OF THE EXPERIMENTAL RESULTS AND CONCLUSIONS

Theoretical expectations described in the previous sections can be separated into the qualitative and quantitative predictions. Verification of the qualitative prediction of the orbital mechanism of a large negative magnetoresistance in the variable-range hopping regime is relatively simple: it requires measurements of the anisotropy with respect to the parallel and perpendicular magnetic field. By contrast, verifying quantitative predictions represented by (18) and (19) would require stronger conditions $\ln[\varrho(0)/\rho(B)] > 1$ and $B\xi^2 > \Phi_0$. We are not aware of experiments on the negative magnetoresistance where all these requirements were satisfied. Below, we discuss the currently available data on large negative magnetoresistance in the variable-range hopping.

We begin with the maximal value of the magnetoresistance observed experimentally and expected theoret-

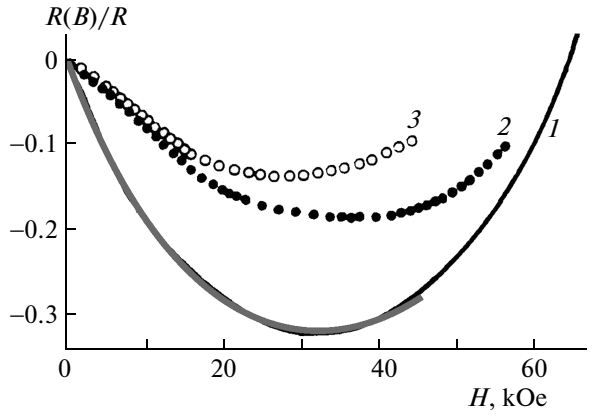

Fig. 16. Data from [8] and their fit to the behavior in (18) expected for relatively small resistances $R_\square/R_Q \approx 10^3$–$10^4$ involving the matrix elements computed in Sec. 3.2. Curve *1* corresponds to the field perpendicular to the plane of the sample. Data points *2* show the effect of the field in the plane of the sample perpendicular to the direction of the current, and data set *3* — to the field in the direction of the current. The gray line shows the theoretical expectations. The upturn at large fields is due to the effect of the field at small scales, where it modifies the hopping amplitude between the sites, which was not taken into account properly in the model

ically. In our numerical simulations, we obtained the maximum value $\delta\xi/\xi = 0.2$ for the uniform density of states (Mott regime) and $\delta\xi/\xi = 0.05$ for the density of states linear in ε (Efros–Shklovskii regime). The measurable values of the resistance ($R \lesssim 10^{11}\,\Omega$) correspond to $(T_0/T)^\zeta \lesssim 15$. Hence, Eqs. (18) and (19) describe the negative magnetoresistance whose value does not exceed $\varrho\,(0)\,/\rho\,(B) < 30$ in the Mott regime, and is expected to be more moderate, $\ln[\rho\,(0)\,/\rho\,(B)] < 1$, in Efros–Shklovskii regime. This is in agreement with the fact that in all papers [8–18] where both the large negative magnetoresistance has been observed and the temperature dependence of the resistance has been measured, it followed Mott's law.

Surprisingly, one of the most comprehensive studies of the negative magnetoresistance in the variable-range hopping regime in a two-dimensional material was done in the early work [8] that studied Ge-sopped GaAs films. It observed a strongly anisotropic negative magnetoresistance, the largest one corresponding to the out-of-plane field. The effect of the in-plane field can be accounted for by a significant thickness of the film ($d_{eff} \approx 30$ nm). Moreover, the in-plane negative magnetoresistance was also anisotropic with respect to the angle between the magnetic field and the current. Finally, microscopic fluctuations of the resistance as a function of the magnetic field in small samples were observed. These observations prove the orbital nature of the effect. In this experiment, the resistance of the sample was $R_\square \lesssim 30$ MΩ at lowest temperatures, indicating that $r/\xi \lesssim 5$. Accordingly, the magnitude of the negative magnetoresistance remained moderate: $((\rho\,(0) - \rho\,(B))\,/\rho\,(0))_{max} \approx 0.4$. In Fig. 16, we present results of our numerical simulations of Eq. (26) and their comparison with the experimental data in [8]. Paper [10] observed negative magnetoresistance with a similar amplitude and a similar dependence on the magnetic field in thin films of polycrystalline In_2O_{3-x}.

A subsequent paper [9] on $GaAs/Al_xGa_{1-x}As$ disordered heterojunctions observed the significantly larger negative magnetoresistance $\varrho(0)/\rho(B) \approx 7$. Strong anisotropy of the negative magnetoresistance has been observed, indicating the orbital nature of the effect. The magnetic field dependence of $\rho(B)$ in low fields $B \lesssim 4$ T where magnetoresistance is negative was roughly linear in coordinates $\ln\rho(B)$, $B^{1/2}$, which is in good agreement with the dependence expected theoretically (25) and shown in Fig. 14. In these experiments, the localization length ξ varied in the range 25–100 nm for different gate voltages, with $B\xi^2 \sim \Phi_0$ occurring at $B \sim 4$ T. Generally, one expects that the magnetoconductance should show a crossover to a different regime when $B\xi^2 \sim \Phi_0$. It is surprising that this crossover is not observed in the data. On the other hand, this paper and the papers discussed below give values for the localization length ξ extracted from the Mott law. This procedure is prone to a number of uncertainties such as the value of the density of states, the exact form of the temperature dependence, etc., and the values of the localization length might therefore be wrong by a factor 2–5, which would be sufficient to explain the absence of the crossover in [9]. A similar large negative magnetoresistance ($\varrho(0)/\rho(B) \approx 20$) of the orbital nature was observed in polycrystalline In_2O_{3-x} films in [1]. The behavior of $\varrho(0)/\rho(B)$ in these experiments resembles a small power of magnetic fields in a wide range of fields for all fields; the quadratic behavior was observed only in very low fields ($B < 0.2$ T), at which the relative change in the resistance was very small, $\delta R/R \ll 1$, in agreement with the theoretical expectations (cf. Fig. 13 in which the B^2 behavior appears at $\delta R/R \lesssim 10^{-2}$–$10^{-1}$).

The maximal value of magnetoresistance in [9–11] is somewhat above the value expected theoretically for the films of these resistances. For instance, the resistance of $GaAs/Al_xGa_{1-x}As$ films in [9] implies that at

the lowest temperature, the maximal value for these films is $(T_0/T)^{1/3} \approx 7$, which translates into the maximal expected value $\rho(0)/\rho(B) \approx 2$–$3$. It is possible, however, that the largest fields studied in these papers correspond to the regime $B\xi^2 \gtrsim \Phi_0$, in which the magnetoresistance may continue to grow with B.

A huge effect of the transverse field on the conductivity ($\varrho(0)/\varrho(B) \gtrsim 30$) of high mobility silicon MOSFET was observed [12, 13] at low carrier concentrations. Remarkably, the large magnetoresistance in the transverse field appears in these experiments only when the spins are polarized by a large in-plane field, while low fields result in an isotropic small and positive magnetoresistance. The latter indicates the spin nature of the magnetoresistance, which is in agreement with the strong correlations expected in this material. As discussed in Sec. 3.3, this implies the existence of localized spins in the system that suppress the orbital effect of the magnetic field. Application of a large in-plane field polarizes the spins, making the path interference possible, such that a transverse field added to the system leads to a large negative magnetoresistance, as is observed experimentally. Unfortunately, paper [12] did not study the temperature dependence of the resistivity in these samples. It is likely that the change of the sign of magnetoresistance observed in [14] in studying the pregraphitic carbon nanofibers that obey the Efros–Shklovskii law is due to a similar mechanism. Unfortunately, this work did not study the field anisotropy.

Paper [15] reported a big negative magnetoresistance ($\varrho(0)/\varrho(B) \sim 10$) of H-doped graphene, while the in-plane field had practically no effect on the resistance. The observed negative magnetoresistance can be interpreted as a large change in the localization length $\xi(B)/\xi(0) = 4$ induced by the field $B = 9\,\mathrm{T}$. These results cannot be compared directly with the universal scaling dependence derived in this paper because the large changes in the localization length imply that $B\xi^2 \sim 1$. We expect that at lower temperatures, the samples studied in this work should exhibit large magnetoresistance at low fields associated with small $\delta\xi/\xi$, but these data are not available.

Finally, it is possible that negative magnetoresistance due to the orbital effect was also observed in other materials but was not studied in any detail. For instance, a sharp (factor of 2) drop of the resistance in the fields $B = 1\,\mathrm{T}$ at $T = 100\,\mathrm{mK}$ was observed in [16] for CdSe: in samples that display the three-dimensional Mott resistance with the exponent $\zeta = 1/4$ and $R(0) = 6\ \mathrm{M\Omega \cdot cm}$, significant ($\delta G/G \approx 0.2$) negative magnetoresistance was also observed in three-dimensional doped n-type InP samples that also show the Mott law but a much lower resistance $R(0) \sim 10\,\Omega \cdot \mathrm{cm}$. Paper [17] reported a decrease in the resistance by a factor of 100 in the field $B = 1$ T for Ge films at $T = 36\,\mathrm{mK}$ characterized by $R = 400\ \mathrm{k\Omega}$.

The complexity of the data outlined above shows that they cannot be explained solely by a single-particle theory. In particular, it cannot explain why some materials exhibit only positive while others only negative magnetoresistance in the whole range of temperatures and magnetic fields in the variable-range hopping regime. Moreover, there are also materials that exhibit an isotropic positive magnetoresistance only at small fields. At larger in-plane fields, the magnetoresistance of these samples saturates, and addition of a small perpendicular field results in a giant negative magnetoresistance [12, 13]. Evidently, the spin physics plays an important role in the these materials.

Positive magnetoresistance of several orders of magnitude in high magnetic fields has been observed in many experimental works (see, e. g., [23, 48, 49]). However, no data set is sufficiently complete to allow associating it with the orbital interference mechanisms [19] described by (18) and (19). For example, these works did not study the anisotropy of the magnetoresistance.

We now briefly discuss the origin of the isotropic positive magnetoresistance in small fields, which was observed in a number of works. There are at least three possibilities. The first is that the electron spin polarization increases the electron energy. As a result, the density of states at the Fermi energy changes as well. This is expected to be a relatively small effect. An alternative mechanism associates it with the presence of both singly and doubly occupied states near the Fermi energy in the impurity band. In the absence of a magnetic field, the process in which the electron hops from one occupied site to another (creating a singlet) is possible. The magnetic field polarizes spins, which suppresses such processes [50]. Thus, the magnetic field effectively changes the density of states in the impurity band. This mechanism provides contribution to $\log\sigma$ that are quadratic in B. Therefore, it can be effective only in the absence of the orbital contribution, which is nonanalytic in B.

A different mechanism might be effective if the electron system is strongly correlated and in the absence of disorder is close to the Wigner-crystal–Fermi-liquid transition. In the presence of disorder, the system may be visualized as a random mixture of crystal and liquid puddles. In this case, the insulating phase corresponds to the situation where metallic puddles do not overlap. Because the magnetic susceptibility of the Wigner crystal is higher than that of the Fermi liquid, the frac-

tion of the Wigner crystal grows with increasing the magnetic field, leading to the positive magnetoresistance [13]. In the theory of ^{3}He, this phenomenon is known as the Pomeranchuk effect. It is possible that the huge positive isotropic magnetoresistance observed in [12, 13, 51] in the metallic regime of Si MOSFET's and GaAs quantum wells is due to this mechanism. We believe that the same mechanism may be responsible for the positive isotropic magnetoresistance in the hopping regime [13].

Finally, the spin alignment in the parallel field produces the interference between the paths and corresponds to a new mechanism of magnetoresistance. Although this mechanism in the hopping regime has never been considered theoretically, it is clear that it also produces a negative magnetoresistance. We expect that this contribution will be isotropic.

While this work was in progress, we learned about paper [52] that gives the arguments for the universal corrections to the magnetoresistance of strongly disordered superconductors described by a model similar to the electron hopping discussed here. In our terminology, this model corresponds to the case of the uniform density of states and positive scattering amplitudes.

We acknowledge useful discussions with M. Feigelman, J. Folk, X. P. A. Gao, M. Gershenson, D. Huse, S. Kravchenko, I. Sadovskyy, M. Sarachik, and B. I. Shklovskii. B. S. thanks the International Institute of Physics (Natal, Brazil) for the hospitality during the completion of the paper. This research was supported by grants ARO W911NF-09-1-0395, ANR QuDec, and John Templeton Foundation. The opinions expressed in this publication are those of the authors and do not necessarily reflect the views of the John Templeton Foundation and Templeton.

REFERENCES

1. A. L. Efros and B. I. Shklovskii, in *Modern Problems in Condensed Matter Sciences. Electron-Electron Interactions in Disordered Systems*, ed. by A. Efros and M. Pollak, North-Holland (1985), Vol. 10, ch. 5, p. 409.

2. N. F. Mott, *Metal-insulator Transitions*, Taylor and Francis (1990).

3. A. A. Abrikosov, *Fundamentals of the Theory of Metals*, North-Holland (1988).

4. B. L. Altshuler, P. A. Lee, D. Khmel'nitzkii, and A. I. Larkin, Phys. Rev. B **22**, 5142 (1979), URL http://dx.doi.org/10.1103/PhysRevB.22.5142.

5. S. Hikami, A. I. Larkin, and Y. Nagaoka, Progr. Theor. Phys. **63**, 707 (1980).

6. A. I. Larkin, Pis'ma v Zh. Eksp. Teor. Fiz. **31**, 239 (1980) [JETP Lett. **31**, 219 (1980)].

7. P. A. Lee and T. V. Ramakrishnan, Rev. Mod. Phys. **57**, 287 (1985), URL http: //dx.doi.org/10.1103/ /RevModPhys.57.287.

8. E. I. Laiko, A. O. Orlov, A. K. Savchenko, E. A. Il'ichev, and E. A. Poltoratskii, Zh. Eksp. Teor. Fiz. **93**, 2204 (1987) [JETP **66**, 1258 (1987)].

9. H. W. Jiang, C. E. Johnson, and K. L. Wang, Phys. Rev. B **46**, 12830 (1992), URL http://dx.doi.org/ /10.1103/PhysRevB.46.12830.

10. F. P. Milliken and Z. Ovadyahu, Phys. Rev. Lett. **65**, 911 (1990), URL http://dx. doi.org/10.1103/ /PhysRevLett.65.911.

11. A. Frydman and Z. Ovadyahu, Sol. St. Comm. **94**, 745 (1995), URL http: //dx.doi.org/10.1016/ /0038-1098(95)00141-7.

12. S. V. Kravchenko, D. Simonian, M. P. Sarachik, A. D. Kent, and V. M. Pudalov, Phys. Rev. B **58**, 3553 (1998), URL http://dx.doi.org/10.1103/ /PhysRevB.58.3553.

13. B. Spivak, S. V. Kravchenko, S. A. Kivelson, and X. P. A. Gao, Rev. Mod. Phys. **82**, 1743 (2010), URL http://dx.doi.org/10.1103/RevModPhys.82.1743.

14. Y. Wang and J. J. Santiago-Aviles, Appl. Phys. Lett. **89**, 123119 (2006), URL http://dx.doi.org/10.1063/ /1.2338573.

15. X. Hong, S.-H. Cheng, C. Herding, and J. Zhu, Phys. Rev. B **83**, 085410 (2011), URL http://dx.doi.org/10.1103/PhysRevB.83.085410.

16. J. R. Friedman, Y. Zhang, P. Dai, and M. P. Sarachik, Phys. Rev. B **53**, 9528 (1996), URL http://dx.doi.org/ /10.1103/PhysRevB.53.9528.

17. V. F. Mitin, V. K. Dugaev, and G. G. Ihas, Appl. Phys. Lett. **91**, 202107 (2007), URL http://dx.doi.org/ /10.1063/1.2813615.

18. F. Hellman, M. Q. Tran, A. E. Gebala, E. M. Wilcox, and R. C. Dynes, Phys. Rev. Lett. **77**, 4652 (1996), URL http://dx.doi.org/10.1103/PhysRevLett.77.4652.

19. B. I. Shklovskii, Zh. Eksp. Teor. Fiz. **84**, 811 (1983) [JETP Lett. **36**, 51 (1982)].

20. B. I. Shklovskii and A. L. Efros, Zh. Eksp. Teor. Fiz. **85**, 721 (1983) [JETP **57**, 470 (1983)].

21. A. V. Khaetskii and B. I. Shklovskii, Pis'ma v Zh. Eksp. Teor. Fiz. **36**, 43 (1982) [JETP **58**, 421 (1983)].

22. B. I. Shklovskii, Sov. Phys. Semiconductors **17**, 1311 (1983).

23. B. I. Shklovskii and A. L. Efros, *Electronic Properties of Doped Semiconductors*, Springer (1984).

24. V. L. Nguen, B. Z. Spivak, and B. I. Shklovskii, Zh. Eksp. Teor. Fiz. **89**, 1770 (1985) [JETP **62**, 1021 (1985)].

25. B. I. Shklovskii and B. Z. Spivak, in *Hopping and Related Phenomena*, World Sci. Singapore (1990), p. 139.

26. E. Medina, M. Kardar, Y. Shapir, and X. R. Wang, Phys. Rev. Lett. **64**, 1816 (1990), URL http://dx.doi.org/10.1103/PhysRevLett.64.1816.

27. B. I. Shklovskii and B. Z. Spivak, in *Modern Problems in Condensed Matter Sciences. Hopping Transport in Solids*, ed. by M. Pollak and B. Shklovskii, Elsevier (1991), Vol. 28, ch. 9, p. 271.

28. H. L. Zhao, B. Spivak, M. P. Gelfand, and S. Feng, Phys. Rev. B **44**, 10760 (1991), URL http://dx.doi.org/10.1103/PhysRevB.44.10760.

29. V. L. Nguen, B. Z. Spivak, and B. I. Shklovskii, Pis'ma v Zh. Eksp. Teor. Fiz. **43**, 35 (1986) [JETP Lett. **43**, 44 (1986)].

30. B. I. Shklovskii and B. Z. Spivak, J. Stat. Phys. **38**, 267 (1985).

31. E. Medina and M. Kardar, Phys. Rev. B **46**, 9984 (1992), URL http://link.aps.org/doi/10.1103/PhysRevB.46.9984.

32. E. Medina, M. Kardar, and R. Rangel, Phys. Rev. B **53**, 7663 (1996), URL http://dx.doi.org/10.1103/PhysRevB.53.7663.

33. H. Kim and D. A. Huse, Phys. Rev. B **83**, 052405 (2011), URL http://dx.doi.org/10.1103/PhysRevB.83.052405.

34. D. Huse and C. Henley, Phys. Rev. Lett. **54**, 2708 (1985), URL http://dx.doi.org/10.1103/PhysRevLett.54.2708.

35. M. Kardar and Y.-C. Zhang, Phys. Rev. Lett. **58**, 2087 (1987), URL http://dx.doi.org/10.1103/PhysRevLett.58.2087.

36. M. Kardar, Nucl. Phys. B **290**, 582 (1987).

37. V. S. Dotsenko, L. B. Ioffe, V. B. Geshkenbein, S. E. Korshunov, and G. Blatter, Phys. Rev. Lett. **100**, 050601 (2008), URL http://dx.doi.org/10.1103/PhysRevLett.100.050601.

38. M. Kardar, D. Huse, C. Henley, and D. Fisher, Phys. Rev. Lett. **55**, 2923 (1985), URL http://dx.doi.org/10.1103/PhysRevLett.55.2923.

39. M. Kardar and D. Nelson, Phys. Rev. Lett. **55**, 1157 (1985), URL http://dx.doi.org/10.1103/PhysRevLett.55.1157.

40. M. Kardar, G. Parisi, and Y. C. Zhang, Phys. Rev. Lett. **56**, 889 (1986), URL http://dx.doi.org/10.1103/PhysRevLett.56.889.

41. P. Calabrese, P. Le Doussal, and A. Rosso, Europhys. Lett. **90**, 20002 (2010), URL http://dx.doi.org/10.1209/0295-5075/90/20002.

42. V. Dotsenko, Europhys. Lett. **90**, 20003 (2010), URL http://dx.doi.org/10.1209/0295-5075/90/20003.

43. C. Tracy and H. Widom, Comm. Math. Phys. **159**, 151 (1994).

44. A. Somoza, M. Ortuno, and J. Prior, Phys. Rev. Lett. **99**, 116602 (2007), URL http://dx.doi.org/10.1103/PhysRevLett.99.116602.

45. J. Prior, A. Somoza, and M. Ortuno, Europ. Phys. J. B **70**, 513 (2009), URL http://dx.doi.org/10.1140/epjb/e2009-00244-x.

46. R. N. Bhatt and P. A. Lee, Phys. Rev. Lett. **48**, 344 (1982), URL http://dx.doi.org/10.1103/PhysRevLett.48.344.

47. K. H. Fischer and J. A. Hertz, *Spin Glasses*, Cambridge Univ. Press, Cambridge (1993).

48. I. Shlimak, A. Ionov, and B. I. Shklovskii, Sov. Phys. Semicond. **17**, 314 (1983).

49. A. N. Ionov, I. S. Shlimak, and M. N. Matveev, Sol. St. Comm. **47**, 763 (1983), URL http://dx.doi.org/10.1016/0038-1098(83)90063-7.

50. H. Kamimura, in *Modern Problems in Condensed Matter Sciences. Electron-Electron Interactions in Disordered Systems*, ed. by A. Efros and M. Pollak, North-Holland (1985), Vol. 10, ch. 7, p. 555.

51. X. P. A. Gao, G. S. Boebinger, A. P. Mills, A. P. Ramirez, L. N. Pfeiffer, and K. W. West, Phys. Rev. B **73**, 241315 (2006), URL http://dx.doi.org/10.1103/PhysRevB.73.241315.

52. A. Gangopadhyay, V. Galitski, and M. Mueller, arXiv:1210.3726.